

J.-P. Boulanger · C. Menkes

The Trident Pacific model. Part 2: role of long equatorial wave reflection on sea surface temperature anomalies during the 1993–1998 TOPEX/POSEIDON period

Received: 28 May 1999 / Accepted: 18 May 2000

Abstract The present study aims to give a quantitative description of the role played by long equatorial waves on sea surface temperature anomalies during the 1993–1998 TOPEX/POSEIDON period and more specifically during the 1997–1998 El Niño using a new Pacific Ocean model called Trident. In a companion paper, the Trident dynamical component was described and validated with observations. Briefly, the model exhibits skill in simulating not only sea level but also surface zonal current variability in the equatorial wave guide. Here the model thermodynamics are described and validated. The thermodynamics of Trident consist of one single equation for interannual sea surface temperature anomalies. Compared to other similar models, the introduction in the temperature equation of a term equivalent to a vertical mixing term improves significantly the temperature simulations in the eastern Pacific. Thus the model comparison to interannual sea level, zonal current and sea surface temperature anomalies is fairly good over the entire equatorial Pacific Ocean. The model is found to be sensitive to both subsurface variability (central and eastern Pacific) and to zonal current advection, especially near the dateline where the data suggest that advection is a first order process for determining sea surface temperature changes. The role of long equatorial wave reflection observed in TOPEX/POSEIDON data is studied by either cancelling the eastern boundary or western boundary reflection. First, at the eastern boundary, although the reflected Rossby waves were found to act against the warming during the onset phase of the 1997–1998 El Niño through zonal advection, the major impact of these reflected Rossby waves was to reinforce the deepening of the thermocline in the eastern

Pacific initiated by the impinging Kelvin waves. Therefore, all things considered, the Rossby waves strongly contributed to the warming in 1997–1998 east of 120°W. Secondly, at the western boundary, Rossby wave reflection acted as suggested by the delayed action oscillator theory: the reflected Kelvin waves caused shoaling of the thermocline in the central and eastern Pacific where they weakened the warm or cold conditions observed in the Pacific Ocean. During the 1997–1998 event specifically, they contributed to about a third of the upwelling Kelvin wave amplitude propagating in the central Pacific. The other two thirds of the amplitude were found to be actually wind-forced, strongly suggesting that during that event easterly wind anomalies in the western Pacific played a significant role in the termination of the recent 1997–1998 El Niño event and its switch to the La Niña period.

1 Introduction

The development of the observational networks over the tropical Pacific Ocean such as the Tropical Ocean Global Atmosphere – Tropical Atmosphere Ocean Array (Hayes et al. 1991; McPhaden 1993), the thermal profile measurements by expendable BathyThermograph sondes, and various satellites (e.g. TOPEX/POSEIDON measuring sea-level, ERS measuring winds) provide for the first time the opportunity to observe, describe and understand the mechanisms involved in a strong El Niño/Southern Oscillation phenomenon such as the 1997–1998 event. Focusing on the oceanic processes potentially at work during ENSO, two theories (the delayed action oscillator, Schopf and Suarez 1988; Battisti 1988; Mantua and Battisti 1994, and a revised theory, Picaut et al. 1997) are based on the dynamical and thermodynamical changes induced by long equatorial waves. In the former (the delayed action oscillator), the reflection of Rossby waves at the western boundary is a crucial process in terminating a warm event via the thermocline displacements in the eastern Pacific. In the

J.-P. Boulanger (✉) · C. Menkes
Laboratoire d'Océanographie Dynamique et de Climatologie,
UMR CNRS/ORSTOM/UPMC,
Université Pierre et Marie Curie, Tour 26/Etage 4/Case100,
4 Place Jussieu, 75252 Paris, Cedex 05, France
E-mail: jpb@lodyc.jussieu.fr

latter, the reflection of Kelvin waves into Rossby waves at the eastern boundary plays a major role in the displacement of the eastern edge of the warm pool (highly correlated to the Niño3 index) through zonal advection. This displacement induces a feedback on the coupled system through the displacement of the atmospheric response, located mainly to the west of the eastern edge of the warm pool (Picaut et al. 1996). While the former highlights the major role of vertical processes (thermocline displacement) in the central and east Pacific, the latter is based on the important role played by equatorial zonal surface currents via zonal advection in the central and western Pacific.

Recently, Boulanger and Menkes (1999), McPhaden (1999) and McPhaden and Yu (1999) described the variability in the equatorial Pacific during the 1997–1998 El Niño period. In particular, Boulanger and Menkes (1999) offered the following qualitative description of the warm event. First, although the westerly wind event in December 1996 affected slightly the equatorial conditions, the timing of the onset of the El Niño event seemed to be strongly related to the March 1997 westerly wind event located in the western Pacific. The ocean responded by forcing a strong downwelling Kelvin wave which seemed to have contributed to the initiation of positive sea surface temperature anomalies in the far eastern Pacific, and to the eastward displacement of the eastern edge of the warm-pool. Subsequently, westerly wind anomalies shifted to the central Pacific, forcing large downwelling Kelvin waves which propagated to the eastern Pacific and reflected into Rossby waves. Although these reflected Rossby waves seemed to have contributed to a weak westward displacement of the 28 °C isotherm in SST, the positive sea surface temperature anomalies grew larger and the entire equatorial Pacific experienced temperatures higher than 28 °C. At the western boundary, upwelling Rossby waves reflected into upwelling Kelvin waves. Strengthened by easterly wind anomalies observed in the western Pacific in early 1998, this upwelling Kelvin signal was suggested to play a major role in the switch in the temperature anomalies from positive to negative in the central and eastern Pacific leading later to the development of a cold period.

The objective of the present study is to give a quantitative description of the processes involved during the 1997–1998 period by understanding the mechanisms by which long equatorial waves contributed to the observed ENSO variability. In the first part (Boulanger 2000, this issue), the oceanic dynamics of the Trident model have been described and validated using a variety of observations of the tropical Pacific Ocean. The model has three layers: a surface layer of constant depth and two subsurface active layers (i.e. two baroclinic modes). Fluxes of momentum and mass are only allowed between the surface layer and the first subsurface layer. The model comparison to various data sets such as TOPEX/POSEIDON sea level and TAO zonal current data revealed model skill in the simulation of both sea level and surface currents in the equatorial Pacific

Ocean. Considering the model's ability to simulate surface currents, we are confident in studying and discussing the respective roles (induced by long equatorial waves) of thermocline displacement and zonal advection in regulating sea surface temperature anomalies in the Trident model.

In this second part, the model thermodynamics are presented, and the role of long equatorial wave reflection at both the eastern and western boundaries are examined in the light of the two theories previously discussed. The model thermodynamics consists of one single equation for interannual sea surface temperature anomalies. In comparison with other similar models (Zebiak and Cane 1987; Battisti 1988; Chen et al. 1995; Dewitte 2000), an additional term is taken into account. This term has the form of a vertical mixing term and actually represents both the vertical diffusion of temperature in the surface layer and the effects of entrainment/detrainment not explicitly simulated, as the surface mixed-layer has a constant depth. This new term in the temperature equation contributes to an improvement of the temperature variability in the eastern Pacific.

Section 2 presents various data sets (sea surface temperature from the Climate Analysis Center and expendable Bathythermograph Temperature data set). Section 3 describes the model thermodynamics. Section 4 discusses the model subsurface temperature parametrization and compares the model sea surface temperature anomalies to data during the 1993–1998 period. Section 5 describes the model variability (sea level, zonal current and sea surface temperature anomalies) during the 1996–1998 period. Section 6 discusses the role of long equatorial wave reflection at the eastern and western boundaries on the dynamical and thermodynamical processes during the 1996–1998 period. Finally, Sect. 7 discusses the results and gives some conclusions.

2 Data

Tropical Ocean Atmosphere/Expendable
Bathythermograph (TAO/XBT) data

The TAO/XBT data set is a three-dimensional interpolated data set kindly provided by Neville Smith (Smith 1995; Smith and Meyers 1996). Data are monthly averaged and gridded onto a 2° longitude by 1° latitude horizontal grid and onto a vertical grid identical to the Levitus climatology (Levitus 1982). The period covered extends from January 1980 to December 1998. For the sake of consistency with shorter data sets, climatology is computed over the period 1993–1996 as in Boulanger and Menkes (1999) and Boulanger (2000). Interannual anomalies are computed relative to this period. This data set was also used to compute dynamic height relative to 400 dbar.

Sea surface temperature data

Sea surface temperature data, obtained from the Columbia University web site (<http://ingrid.ldgo.columbia.edu/SOURCES>), were compiled by the NOAA Climate Prediction Center. The period covered by data is January 1970–December 1998. Data originally

on a 2° longitude by 2° latitude are interpolated onto the model grid (2° longitude by 0.5° latitude). A climatology is also computed over the period 1993–1996. Interannual anomalies are computed relative to this period.

3 The model thermodynamics

Thermodynamics equation

The model basin geometry and the model grid are displayed in Boulanger (2000, this issue). The thermodynamic equation is computed on a C-grid with a resolution identical to the oceanic model resolution (2° in longitude, 0.5° in latitude). The temperature grid extends from 131°E to 81°W in longitude and from 20°S to 20°N in latitude.

The computation of sea surface temperature anomalies is performed using a single equation as in Zebiak and Cane (1987). Our representation differs from theirs in that an additional term has been added to the equation representing a vertical mixing of temperature at the base of the model's constant depth mixed-layer (see Appendix A for a discussion on the SSTA equation).

The thermodynamical equation has the following form (where barred quantities represent climatological fields and unbarred quantities interannual anomalies; the climatology used here is the one described in Sect. 4 of Boulanger and Menkes 1999):

$$\partial_t T = -\partial_x[(\bar{T} + T)u] + (\bar{T} + T)\partial_x u \quad (1)$$

$$-\partial_x[\bar{u}T] + T\partial_x \bar{u} \quad (2)$$

$$-\partial_y[(\bar{T} + T)v] + (\bar{T} + T)\partial_y v \quad (3)$$

$$-\partial_y[\bar{v}T] + T\partial_y \bar{v} \quad (4)$$

$$- [M(\bar{w} + w) - M(\bar{w})]\partial_z \bar{T} \quad (5)$$

$$- M(\bar{w} + w)\partial_z T \quad (6)$$

$$+ K_T \partial_z T \quad (7)$$

$$+ A_H \Delta_H T \quad (8)$$

$$- r_T T \quad (9)$$

where $M(x)$ is a function equal to x for x positive and 0 otherwise.

The first four terms of the thermodynamic equation represent the zonal advection of temperature by the anomalous currents, the zonal advection of the anomalous temperature by seasonal currents, the meridional advection of temperature by the anomalous currents, and the meridional advection of the anomalous temperature by seasonal currents, respectively.

The fifth and sixth terms represent the anomalous vertical advection of seasonal temperature and the vertical advection of anomalous temperature, respectively.

Term (7) is equivalent to a vertical mixing term with a maximum value of K_T chosen to be $2.5 \cdot 10^{-5}$ (i.e. for a minimum mean observed mixed-layer depth of 20 m; see Appendix A). The major effect of including Eq. (7), even if it is a crude representation of vertical mixing, is to improve the simulation of sea surface temperature anomalies along the coasts at the eastern boundary and north of the equator to the east of 140°W. Moreover it allows one to simulate the extension of SSTA anomalies north of the equator during a strong El Niño in a region of mean downwelling (i.e. where Eqs. 5 and 6 are usually equal to zero). Various values for K_T have been tested, and we found SSTA simulations to not be significantly affected for maximum values of K_T between $5 \cdot 10^{-5} - 0.5 \cdot 10^{-5}$. When values lower than $0.5 \cdot 10^{-5}$ are considered, SST variability in the eastern Pacific (along the South American coast and north of the equator) weakens in comparisons with observations. For values larger than $5 \cdot 10^{-5}$, SSTA become more dependent on the subsurface temperature parametrization (expressed as function of model sea level variability, see later). For this case all other processes play a relatively negligible role in determining SSTA. This is in disagreement with observations, suggesting that a major role is played by zonal advection in the western and central Pacific in SSTA changes (Picaut et al. 1996). Finally,

considering that the model mixed-layer depth is constant, Eqs. (6) and (7) play similar roles of mixing the temperature at the base of the mixed-layer with the mixed-layer temperature (see Appendix A). Therefore in the following, these two terms are summed and represent the “anomalous vertical process”.

Equation (8) is a horizontal diffusion term with a coefficient identical to the one used in the shear layer equation ($A_H = 2000 \text{ m}^2 \cdot \text{s}^{-1}$ at the equator; see Boulanger and Menkes 1999). Finally Eq. (9) is a friction term applied to the temperature anomalies and is a crude representation of interannual heat fluxes ($r_T = (125 \text{ days})^{-1}$).

4 Subsurface temperature parametrization and model validation

In order to compute Eqs. (5), (6), and (7) we need to define the following terms: the seasonal temperature vertical gradient $\partial_z \bar{T}$ and the anomalous temperature vertical gradient $\partial_z T = (T - T_{sub})/h_{ML}$ where h_{ML} is the mixed-layer and T_{sub} represents subsurface temperature anomalies at the base of the mixed-layer. To compute a subsurface temperature data set, interpolated TAO/XBT fields (Smith 1995; Smith and Meyers 1996) are first used to estimate a mixed-layer depth defined as the depth where the temperature is lower than the surface temperature by 0.5 °C (Wang and McPhaden 1999a, b).

Considering that the model mixed-layer (h_{ML}^{mod}) has a constant depth of 50 m, we construct a subsurface temperature for the model such that the vertical temperature gradient computed over 50 m would be equal to the vertical gradient computed from data (i.e. $(SST^{obs} - T_{sub}^{obs})/h_{ML}^{obs} = (0.5)/h_{ML}^{obs} = (SST^{obs} - T_{sub}^{mod})/h_{ML}^{mod} = (SST^{obs} - T_{sub}^{mod})/50$). It is then straightforward to show that the equivalent subsurface temperature at 50 m is: $T_{sub} = SST - 0.5(50/h_{ML})$ where h_{ML} is the mixed-layer depth computed from TAO/XBT data.

The subsurface temperature data set is first used to compute a seasonal vertical gradient of temperature using the CPC seasonal sea surface temperature data. The mean vertical gradient (Fig. 1a) reaches a maximum (2 °C/50 m) between 100°W and 90°W. It is large along the equator in the eastern Pacific and decreases quickly westward and poleward (although another maximum is found near 10°N at the Costa Rica dome). The variability (Fig. 1b) has similar patterns with minimum values found in spring (not shown) and maximum values found in fall (not shown). The seasonal vertical temperature gradient is used in the following to compute Eq. (5) of the thermodynamics equation.

With the subsurface temperature interannual anomalies at hand, a parametrization has been developed to relate these anomalies to observed sea level anomalies (h) following an approach similar to Zebiak and Cane (1987). The parametrization chosen here has the following form:

$$T_{sub} = T_1 \tan h(h/h_1) \quad \text{if } h < 0$$

$$T_{sub} = T_2 \tan h(h/h_2) \quad \text{if } h > 0$$

The coefficients T_1 and T_2 represent the maximum amplitudes that the subsurface temperature anomalies can reach. The coefficients h_1 and h_2 represent a sea level amplitude. The smaller they are, the smaller a sea level anomaly needs to be for a subsurface temperature anomaly to reach its maximum (T_1 or T_2).

Here different tests were performed to compute the four unknown parameters. In each test, we either used dynamic height anomalies computed from TAO/XBT data over the 1980–1998 period or over the 1993–1998 period or TOPEX/POSEIDON sea level anomalies over the 1993–1998 period (all anomalies are computed relative to the 93–96 mean seasonal cycle). First it was found (not shown here) that when the TAO/XBT data set was used over the entire period, spatial patterns of the four parameters were rather noisy certainly due to insufficient data coverage along the equator prior to the development of the TOGA-TAO Array. Then it appeared that the variability of dynamic height computed from

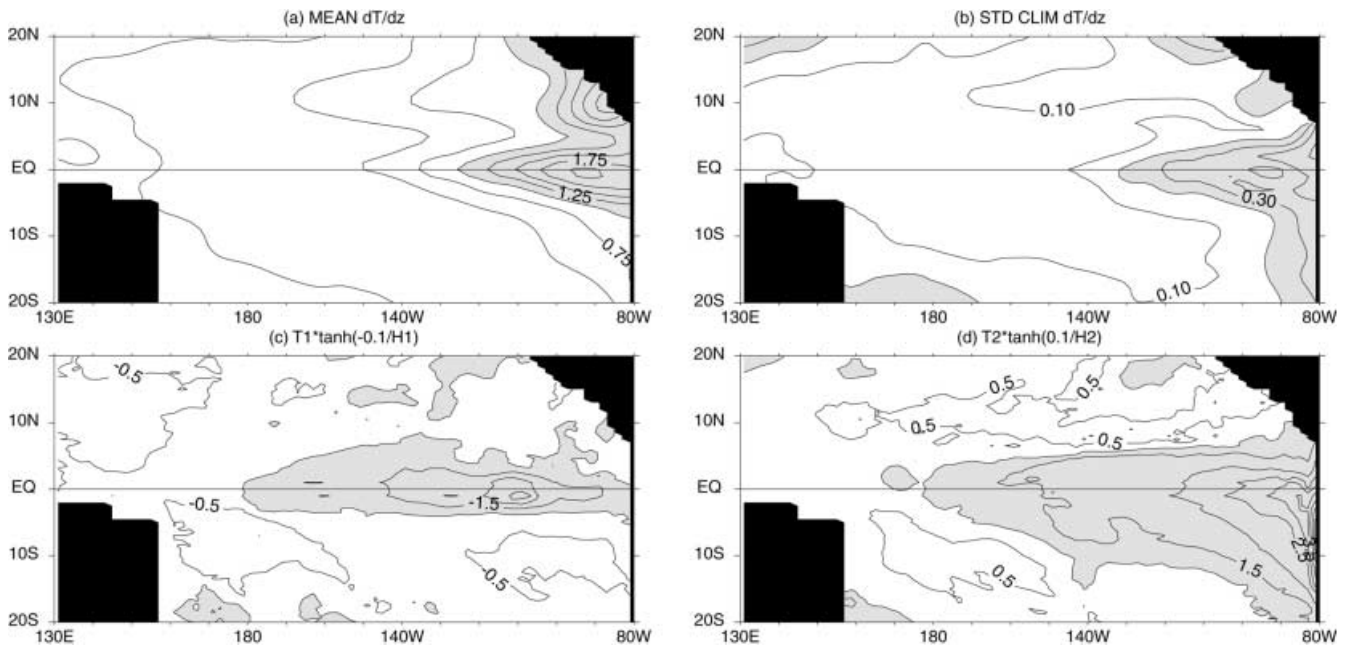


Fig. 1 **a** Mean annual vertical gradient of temperature in $^{\circ}\text{C}/50\text{ m}$ (contours are every $0.25\text{ }^{\circ}\text{C}/50\text{ m}$; values higher than $1\text{ }^{\circ}\text{C}/50\text{ m}$ are shaded); **b** standard deviation of the climatological vertical gradient of temperature in $^{\circ}\text{C}/50\text{ m}$ (contours are every $0.10\text{ }^{\circ}\text{C}/50\text{ m}$; values higher than $0.2\text{ }^{\circ}\text{C}/50\text{ m}$ are shaded); **c** contour intervals for the

subsurface temperature parametrization for a -10 cm sea level anomaly (contours are every $-0.5\text{ }^{\circ}\text{C}$; values lower than $-1\text{ }^{\circ}\text{C}$ are shaded); **d** contour intervals for the subsurface temperature parametrization for a 10 cm sea level anomaly (contours are every $0.5\text{ }^{\circ}\text{C}$; values higher than $1\text{ }^{\circ}\text{C}$ are shaded)

TAO/XBT data especially near the American coasts was weaker than in T/P sea level data. As a consequence and despite the short period under study (6 years), the quality of the T/P data led to the choice of computing the four parameters from T/P sea level anomalies over the period 1993–1998 period. Nevertheless there is no doubt that longer time series will certainly help in improving the subsurface parametrization.

As a first result, when $h < 0$ (Fig. 1c), it appears that for a -10 cm sea level anomaly, the region with the largest response is located near 110°W . However, when $h > 0$, the region with the largest response to a 10 cm sea level anomaly (Fig. 1d) is located near the eastern boundary along the coast and extends westward along the equator.

To evaluate the skill of this parametrization, the parametrized subsurface temperature anomalies are compared to the original data set (Fig. 2). It appears that the two fields are well correlated, especially east of 160°E and west of 170°W in the equatorial wave guide. However the correlation values are smallest near the dateline where it has been suggested (Picaut and Delcroix 1995) that the sea surface temperature anomalies are more likely to be determined by zonal advection. It is thus likely that in this region of usually deep thermoclines the temperature variability at the base of the mixed-layer would be more affected by other processes than vertical processes. On average the rms difference is of the order $0.3\text{ }^{\circ}\text{C}$, with larger values close to the eastern boundary. As a conclusion, the subsurface parametrization represents fairly well the subsurface field especially along the equator and near the eastern boundary where the anomalies are the largest (Fig. 2).

Evaluation of model sea surface temperature anomaly to data

The model was forced during the 1993–1998 period, and model monthly sea surface temperature anomalies were compared to monthly CPC observations (Fig. 3). The model simulates the major patterns of SSTA variability with larger amplitudes in the eastern Pacific and along the South American coast (Fig. 3b). Correlation coefficients are over 0.80 over most of the 5°N – 5°S band, especially in the Niño3 region which is usually considered as a key region for

ENSO variability. However due to the wind forcing, to the model dynamics, to the data with which the parametrization is developed, and to the simplicity of the model parametrizations (including the formulation of heat fluxes), the rms difference between the model and data is larger than $1\text{ }^{\circ}\text{C}$ at the eastern boundary. Finally, the model comparison to the Niño indices (Fig. 4, Table 1) is fairly good, despite some discrepancies in the Niño1+2 index. Correlation coefficients are respectively 0.81, 0.92 and 0.79 in the Niño4, Niño3 and Niño1+2 regions.

5 Interannual variability during the 1996–1998 period

The general features of the observed variability during the 1996–1998 period are quite well reproduced by the Trident model (Fig. 5). The major characteristics of the interannual variability during that period will now be described. In 1996, easterly wind anomalies were located over most of the basin, and they created an east-west gradient with negative sea level anomalies east of the dateline and positive anomalies west of the dateline. Associated with sea level anomalies, westward zonal current anomalies are simulated over most of the basin, and sea surface temperature anomalies are negative to the east of the dateline, while positive anomalies are observed in the western Pacific. Whether these features played a role in “pre-conditioning” the basin for a warm event is a question which will need to be investigated in a coupled mode.

From December 1996 to March 1997, a westerly wind event followed by easterlies and finally by a larger second westerly wind event were observed in the western Pacific. In response to these wind anomalies, large

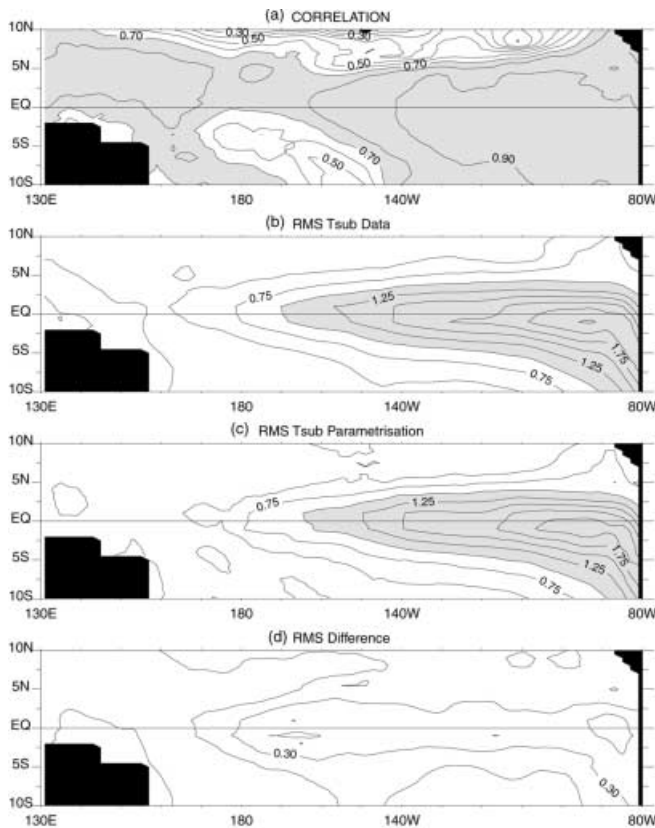


Fig. 2 **a** Map of correlation between TAO/XBT and parametrized subsurface temperature anomalies for January 1993–December 1998 (contour intervals are every 0.1); **b** standard deviation of the TAO/XBT subsurface temperature anomalies (contour intervals are every 0.25); **c** standard deviation of the parametrized subsurface temperature anomalies (contour intervals are every 0.25); **d** Rms difference between the TAO/XBT and parametrized subsurface temperature anomalies over the period January 1993–May (contour intervals are every 0.1)

changes in SSTA (Fig. 6a) are simulated around the dateline due to the displacement of the eastern edge of the warm-pool by zonal advection (Fig. 6b), and thus potentially contributed to the onset of the 1997–1998 El Niño as suggested by Boulanger and Menkes (1999), McPhaden (1999) and Vialard et al. (Submitted 2000). In addition these wind anomalies may have also contributed to the onset of the 1997–1998 through the temperature anomalies they initiated in the eastern Pacific (Fig. 6a) via the role of eastward propagating Kelvin waves on the thermocline depth and the vertical temperature gradient (Fig. 6e). Later, as zonal wind stress anomalies displaced to the central Pacific (Fig. 5a), the eastern Pacific SSTA increased (Figs. 5f, 6a) mainly through a deepening of the thermocline seen as an increase of positive sea level anomalies (Figs. 5b, d, 6e). From August to December 1997, the anomalous zonal advection of total temperature (Fig. 6b) acted to cool the temperature near the dateline, but its effect was mainly counteracted by the climatological zonal advection of anomalous temperature. In total, the role of zonal advection was to contribute to the warming in

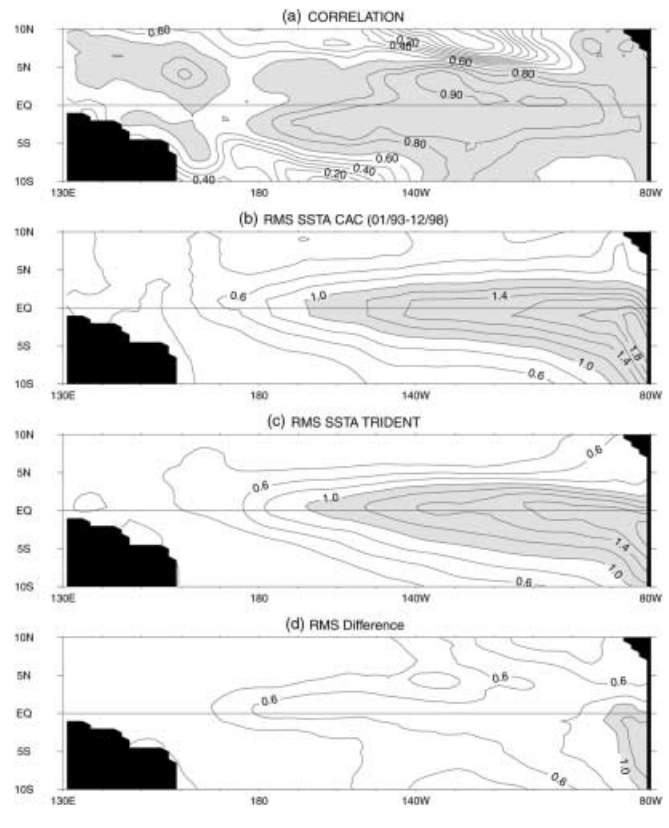


Fig. 3a–d Spatial maps (130°E–80°W/15°S–15°N) of **a** the correlation between the observed and simulated anomalies (contour intervals are every 0.1 from 0. to 0.8, and every 0.05 from 0.80 to 0.95; values higher than 0.7 are shaded); **b** the standard deviation of observed sea surface temperature anomalies (contour intervals are every 0.2 °C and values higher than 1 °C are shaded); **c** the standard deviation of simulated sea surface temperature anomalies (same contours as in **b**), and **d** the rms difference between the observed and simulated anomalies (contour intervals are every 0.2 °C and values higher than 1 °C are shaded)

the central Pacific. During the same period, upwelling Rossby waves propagated westward where they reflected (Boulanger and Menkes 1999). Both reflection and eastward wind anomalies in November 1997 contributed to the large upwelling sea level signal developing in the western Pacific (Fig. 5b–d) which then crossed the basin in 1998. The mechanisms which contributed to the SSTA decrease were (Fig. 6): (1) the feedback term ($-r_T T$), although this term is passive (Fig. 6d); (2) the anomalous vertical processes (Fig. 6e): in particular, in January 1998, from the dateline to 120°W, the strong cooling induced by the vertical advection was responsible for the fast decrease of SSTA; later in May, the switch of SSTA observed around 130°W (Fig. 5c) is partially simulated by the model (Fig. 5f). This switch essentially comes from subsurface cooling processes (Fig. 6e) in response to local wind forcing when westerly wind anomalies weakened in May (Fig. 5a) and upwelling Kelvin waves crossed the basin (Fig. 5d). Such a combination of various dynamical processes is in agreement with the interpretation of McPhaden and Yu (1999). As a first conclusion, although zonal advection played some role

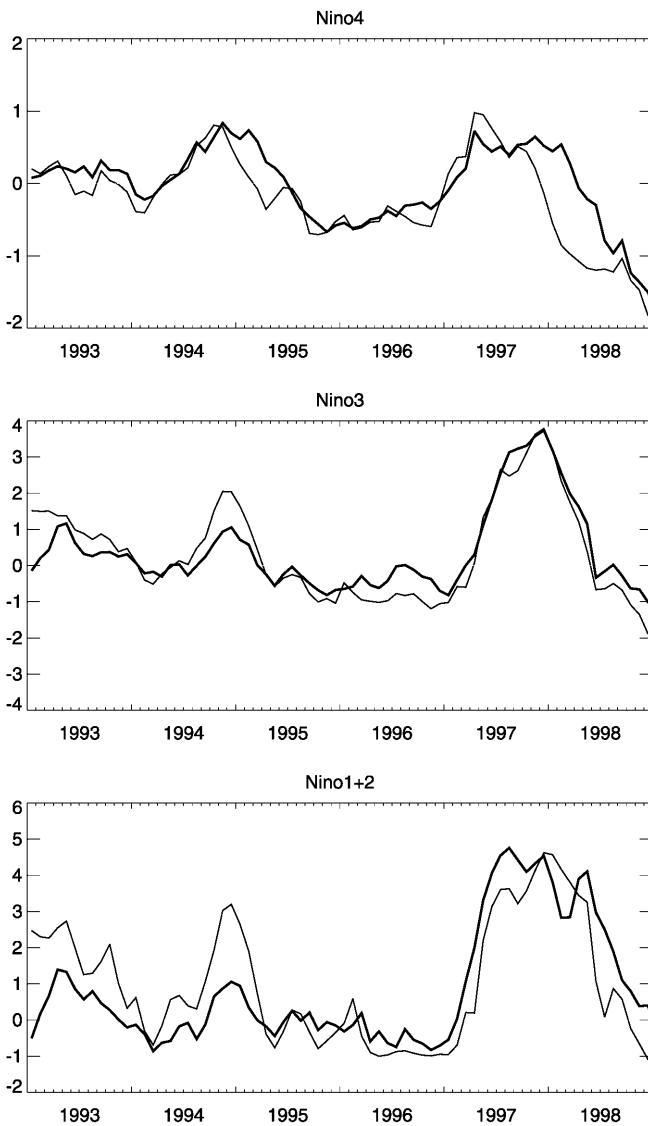


Fig. 4 Time series of the observed (*thick line*) and simulated (*thin line*) sea surface temperature anomalies averaged in the Niño4, Niño3 and Niño1 + 2 boxes. Statistical comparisons are presented in Table 1

Table 1 Evaluation of the simulated SSTA in the different boxes (Niño1 + 2, Niño3, Niño4) to observed indices

	Niño1 + 2	Niño3	Niño4
Correlation	0.79	0.92	0.91
Std data	1.64	1.17	0.55
Std TRIDENT	1.68	1.33	0.60
Rms difference	1.06	0.54	0.35

in the central Pacific, it did not seem to be the major mechanism in the model to reverse the warm anomalies as suggested by Picaut et al. (1997). It appears more likely that this major role was played by the anomalous vertical processes in agreement with Boulanger and Menkes (1999), McPhaden (1999), and McPhaden and Yu (1999). How long equatorial wave reflection con-

tributed to the development and termination of the 1997–1998 El Niño is investigated in the next section.

6 Role of long equatorial wave reflection

Eastern boundary reflection

Boulanger and Menkes (1999) investigated long equatorial wave reflection at the eastern boundary. They showed that these reflections occurred during the entire *T/P* period (1992–1998) with a 75% reflection efficiency. They also argued that the data suggested a decrease in the reflected Rossby signal from the eastern boundary. In order to investigate the role of these reflected Rossby waves, the model was run with no eastern boundary reflection, and the differences between this run and the control run were computed in terms of SLA, ZCA and SSTA (Fig. 7a–c). Large differences in sea level anomalies are observed near the eastern boundaries from which the reflected signal decreases rapidly. Thus a large impact of removing the eastern boundary reflection is to weaken the sea level anomalies in the eastern Pacific as suggested by data (Boulanger and Menkes 1999). However, the reflected Rossby waves are interesting in that their sea level and surface current anomalies tend to act in opposite ways. While the thermocline anomalies reinforce those initiated by impinging Kelvin waves, therefore strengthening the local sea surface temperature anomalies through vertical processes, the zonal current anomalies cancel the Kelvin wave current anomalies and therefore act to push the waters westward (eastward) during an El Niño (La Niña) event. Focusing on the zonal advection process, Picaut et al. (1997) described reflected Rossby waves as a potential contributor to the termination of warm events. Indeed, during the 1997–1998 event, large westward surface currents due to reflected Rossby waves extended far into the eastern and central Pacific as seen in Fig. 7b. However, the major impact on SSTA when reflection is removed at the eastern boundary is through the reduction of thermocline anomalies in the eastern Pacific. Therefore, during the warm event, reflected Rossby waves acted strongly in strengthening the warm anomalies up to 160°W in spring 1998.

Western boundary reflection

Boulanger and Menkes (1999) found reflection to occur during the entire period, although the negative Kelvin wave amplitude in late 1997–early 1998 could not be explained by reflection only. To quantify the actual Kelvin wave amplitude coming from the western boundary reflection, the model is run with no western boundary reflection. The differences between this run and the control run are then computed. In terms of SLA, ZCA and SSTA (Fig. 7d–f), the entire basin is affected in agreement with the basic principles of the delayed

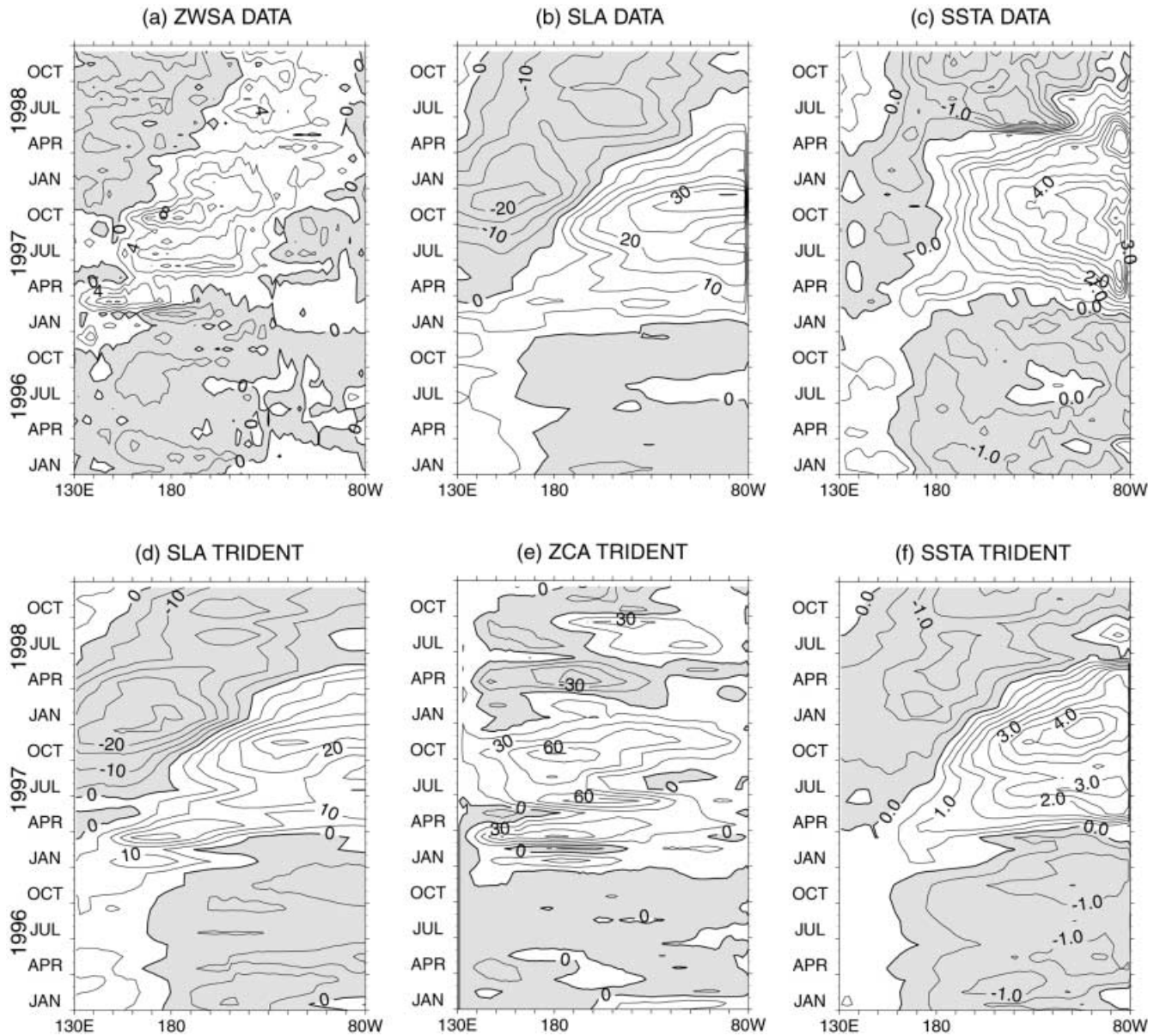


Fig. 5a–f Longitude-time plots of the 2°N–2°S averaged interannual anomalies of **a** ERS+TAO zonal wind stress anomalies in 10^{-2} N/m^2 (contours are every $2 \cdot 10^{-2} \text{ N/m}^2$, negative values are shaded); **b** sea level observed by TOPEX/POSEIDON (contours are every 5 cm, negative values are shaded); **c** observed SSTA (contours are every

0.5 °C, negative values are shaded); **d** simulated sea level anomalies (same contours as **b**); **e** simulated geostrophic zonal currents (contours are every 15 cm/s, negative values are shaded); **f** simulated SSTA (same contours as in **c**)

action oscillator mechanism. The largest differences in the model sea level and zonal current anomalies are in the western Pacific. Focusing on the 1997–1998 period, the western boundary reflection explains up to -8 cm at 150°E when the simulated negative signal is larger than -20 cm . Therefore the reflection explains about one third of the control run signal, and the anomalous easterly winds explain about two thirds of the eastward propagating upwelling Kelvin wave highlighting the major role played by the easterly wind anomalies in the western Pacific in the termination of El Niño (Weisberg and Wang 1997; Harrison and Vecchi 1999). Whether the western boundary reflection is neg-

ligible compared to the effect of wind anomalies in the reversal of the sea surface temperature anomalies from warm to cold will require examination of a coupled model simulation. In terms of surface zonal currents, the reflected Kelvin waves do not contribute significantly to the equatorial surface currents for two reasons. First, as previously stated, a large part of the Kelvin wave is wind-forced in the western Pacific. Second, the Rossby waves which contributed largely to the equatorial zonal currents were not affected significantly by the loss of Kelvin wave amplitude impinging at the eastern boundary. The impact on sea surface temperature anomalies is therefore straightforward: reflected Kelvin

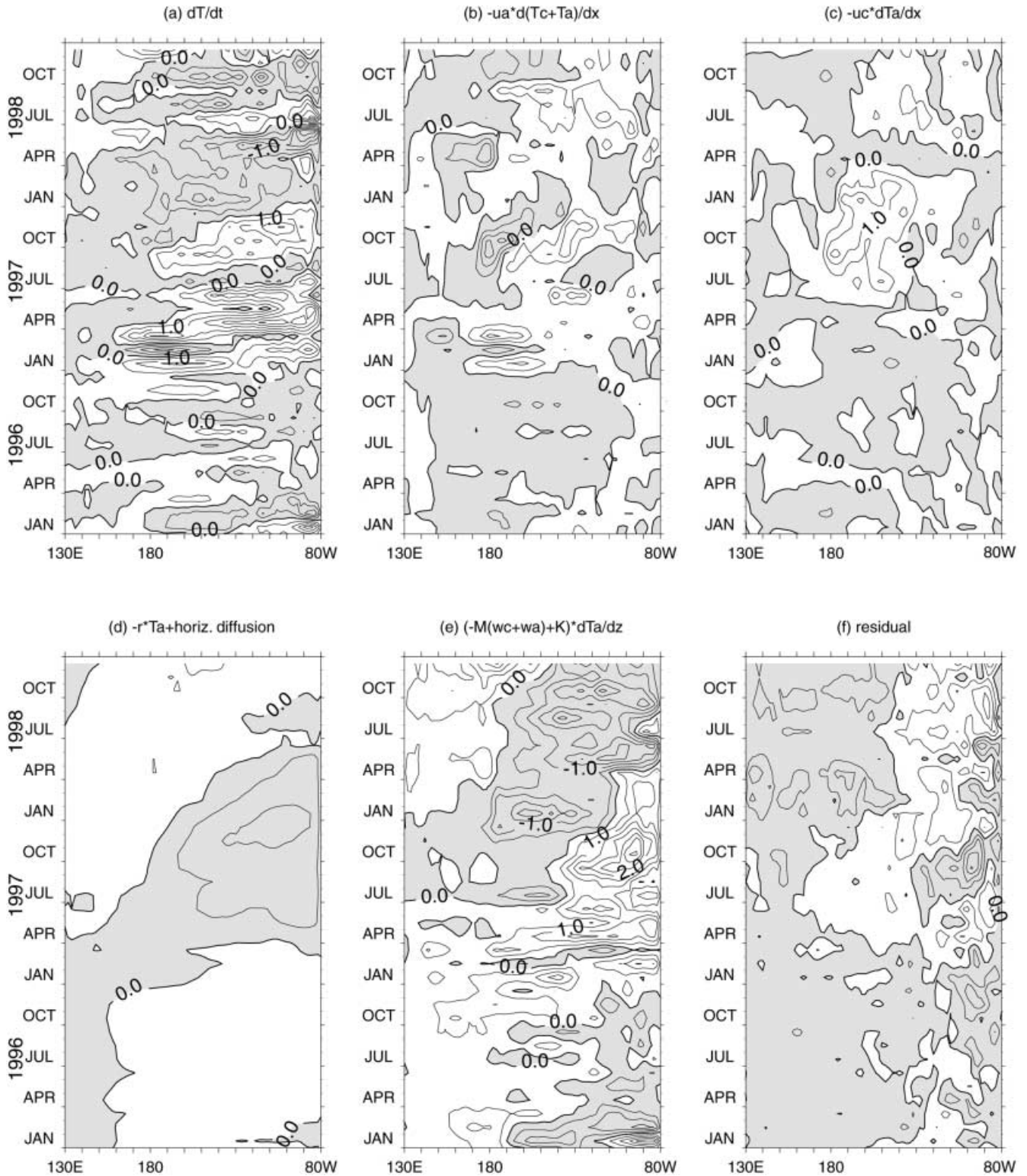


Fig. 6a-f Longitude-time plots of the 2°N – 2°S averaged interannual anomalies of the simulated terms contributing to the sea surface temperature anomaly equation: **a** time derivative, **b** zonal advection by anomalous zonal currents of the total temperature, **c** zonal advection by climatological zonal currents of the temperature anomalies, **d** dissipative terms, **e** vertical advection of the vertical temperature anomalies and vertical diffusivity terms (the sum is

defined as the anomalous vertical process term), **f** residual representing the sum of meridional advection, meridional advection by climatological meridional currents of the temperature anomalies and vertical advection of the climatological subsurface temperature. Contour intervals are every $^{\circ}\text{C}/\text{month}$, negative values are shaded

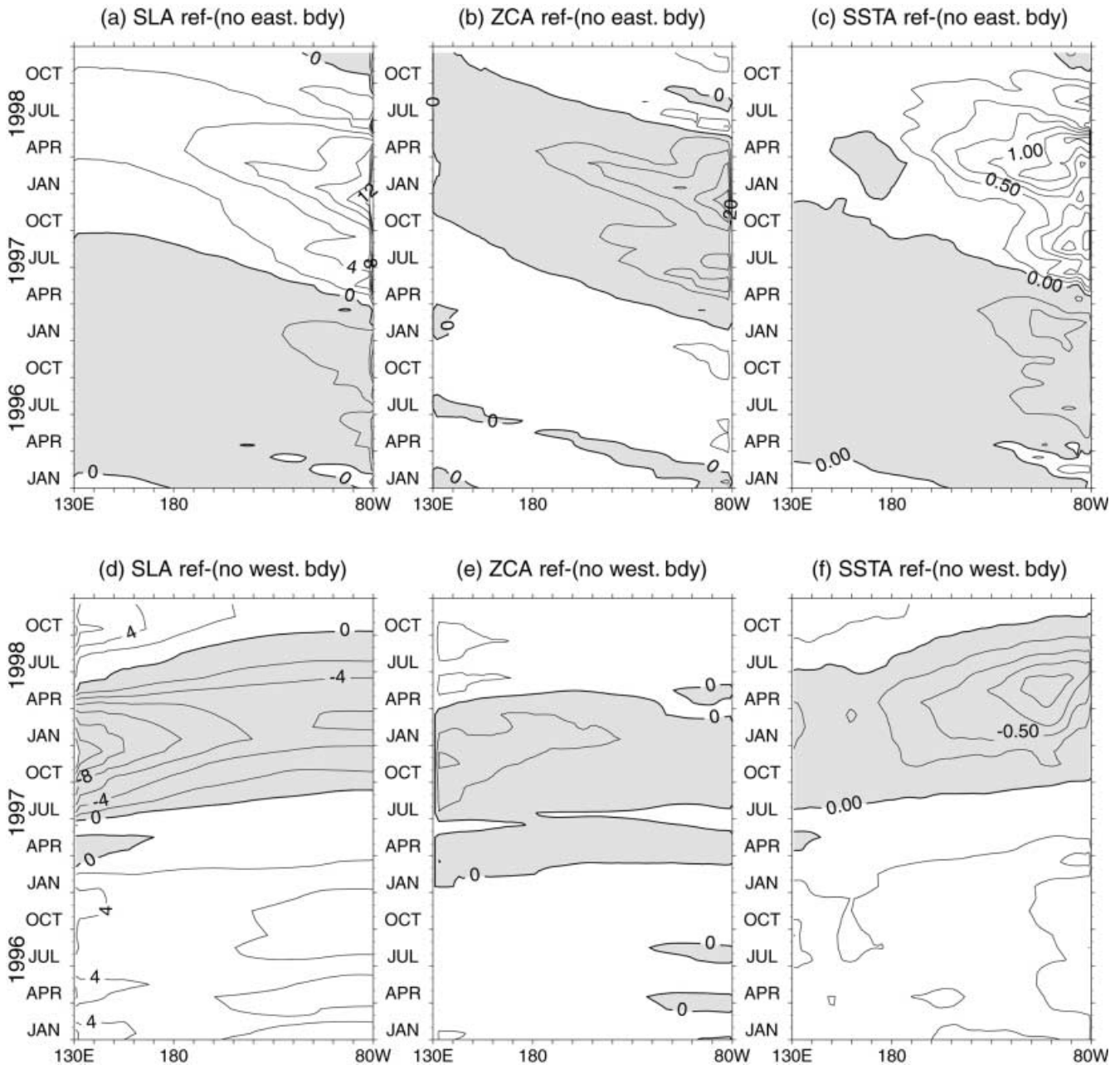


Fig. 7a–f Longitude-time plots of the 2°N–2°S averaged interannual anomalies of: **a–c** differences in sea level, zonal current and sea surface temperature anomalies between the control run and the simulation with no eastern boundary reflection; **d–f** differences in sea level, zonal current and sea surface temperature anomalies between the control

run and the simulation with no western boundary reflection. Contour intervals are respectively every 2 cm for sea level anomalies, every 5 cm/s for zonal current anomalies, and every 0.25 °C for sea surface temperature anomalies. Negative values are shaded

waves tend to cool the ocean when conditions are warm, and to warm the ocean when conditions are cold. This is the basic principle of the delayed action oscillator mechanism. However it is worth noting that the largest negative anomalies (Fig. 7f) are located near the eastern boundary and probably contribute in the model to the switch to cold conditions through vertical processes (Fig. 7g). In data, however, the switch is more abrupt and located at 130°W which suggests that other processes not simulated by linear dynamics may have

taken place (See conclusion of Vialard et al. in press 2000).

7 Discussion and conclusions

In a recent paper, Boulanger and Menkes (1999) investigated long equatorial wave reflection during the 1992–1998 period observed by TOPEX/POSEIDON. They found evidence that the western boundary acted as a

perfect reflector for long first-mode Rossby waves and that the eastern boundary was reflecting Kelvin waves into Rossby waves with a reflection efficiency of 75% of that of an infinite meridional wall. With the existence of boundary reflection at hand, they examined qualitatively the possible existence of the delayed action oscillator mechanism and the revised theory proposed by Picaut et al. (1997) during the 1997–1998 El Niño. Their study led them to the conclusion that although both theories needed to be considered simultaneously to understand the oceanic variability during the 1997–1998 El Niño event, western boundary reflection and wind-forcing in the western Pacific were more likely to explain the decay phase of the warm event. The aim of the present work is to bring a more quantitative estimate of the role of long equatorial waves and their reflection during the strong 1997–1998 warm ENSO.

A preliminary step was to develop a model of the equatorial Pacific basin, which could be used as a reliable tool to understand the role of long equatorial waves through zonal advection and vertical processes. This simple ocean model, named Trident, is composed of a dynamical and a thermodynamical component. Briefly, the dynamical component has been shown (Boulanger 2000, this issue) to exhibit skill in representing sea level variability (T/P sea level data) and equatorial surface currents (TAO surface currents), giving confidence in its use to assess the respective roles of thermocline displacement and zonal advection on SSTA variability.

The model is similar to other simple models (Zebiak and Cane 1987; Battisti 1988; Chen et al. 1995), in that the sea surface temperature interannual anomalies (SSTA) are computed using one single equation and the model assumes a constant mixed-layer depth of 50 m. However the Trident SSTA equation also includes a simplified representation of vertical diffusion at the base of the mixed-layer. Here, for the sake of simplicity we used a time-independent vertical diffusivity coefficient whose spatial structure is a function of the mean mixed-layer computed from TAO/XBT data (see Appendix A). It mainly improves the simulation of SSTA in the eastern Pacific along the coast, and to the north of the equator in the region of downwelling.

The model's interannual anomalies in sea level, zonal currents and sea surface temperature at the equator reproduce observations fairly well (T/P sea level anomalies, and CAC sea surface temperature anomalies). The analysis of the tendency terms in the SST equation shows that the major active contributions to SST changes are the zonal advection and the anomalous vertical process terms. Zonal advection played some role only near the dateline. But the major SST changes in the eastern Pacific are strongly dominated by the anomalous vertical processes especially during the growth and termination of the 1997–1998 El Niño.

These previous comparisons to observations give confidence in using the model to study the role of reflected long equatorial waves during the TOPEX/

POSEIDON period. Thus the model was first run with no eastern boundary reflection. It was shown that during the El Niño event, the reflected Rossby waves may have played two opposing roles. On one hand, they contributed significantly to the downwelling sea level anomalies in the eastern Pacific i.e. they potentially increased the warming initiated by the Kelvin waves through a larger deepening of the thermocline. On the other hand, they created large westward currents which potentially advected the warm waters back to the central and western Pacific. The model shows that the major impact of reflected Rossby waves is found in the eastern Pacific (east of 140°W) where they actually strengthened the warm anomalies by deepening further the thermocline which had already deepened in response to incoming Kelvin waves. The warming was achieved through a vertical process and dominated the potential cooling by zonal advection.

After this the model was run without allowing reflection at the western boundary. The major impact is in agreement with the basic principle of the delayed action oscillator mechanism, as the effect of reflected Kelvin waves on SSTA variations is mainly through a vertical displacement of the thermocline. During the warm 1997–1998 ENSO event, the reflected upwelling Kelvin waves acted in weakening the downwelling signals which were wind-forced in the central Pacific. However, this reflection at the end of the warm period only explains a third of the upwelling Kelvin signal in the western Pacific observed to propagate eastward. Therefore about two thirds of the Kelvin wave amplitude propagating eastward was actually forced by easterly wind anomalies. This result highlights the important role played by the wind-forcing in the western Pacific in the termination of the 1997–1998 El Niño (Harrison and Vecchi 1999), and, possibly, in the reversal to cold La Niña conditions. In the model, the switch from warm to cold conditions is weaker than the abrupt transition observed near 130°W. More complexity in the model SST equation (e.g. time-varying mixed-layer depth) would certainly be required in order to realistically simulate this transition (Vialard et al. 2000).

Acknowledgements The research described in this paper was initiated while Jean-Philippe Boulanger was at the Jet Propulsion Laboratory, California Institute of Technology, under contract with National Aeronautics and Space Administration. It was completed while Jean-Philippe Boulanger was working for Centre National de la Recherche Scientifique at Laboratoire d'Océanographie Dynamique et de Climatologie (LODYC, Jussieu, Paris). We are thankful to the Institut National des Sciences de l'Univers (INSU) and the Programme National d'Etude de la Dynamique du climat (PNEDC) for their financial support as well as to the Centre de Calcul Recherche at Réseau Jussieu (CCR) for providing super computing facilities. The authors thank the Center for Space Research from the University of Texas for providing the processed and gridded TOPEX/POSEIDON data (<http://www.csr.utexas.edu/sst/gpdata.html>), and Neville Smith who kindly made available his subsurface temperature analysis based on TAO/XBT data. The NOAA Climate Prediction Center is also thanked for providing sea surface temperature analyses. Jean-Philippe Boulanger also thanks Lee-Lueng Fu for his constant support, Claire Perigaud for her useful comments, as well as all the people from the Ocean Science Element at JPL who helped

him or with whom he had discussions during his 2-year stay there. Keith A. Rodgers is greatly thanked for his proof-reading comments which considerably helped in improving the English version of the manuscript. The authors also thank Pascale Delecluse, Gurvan Madec, Gilles Reverdin, Jérôme Sirven, Jérôme Vialard and many people from LODYC who contributed to the evolution and design of the Trident model. The comments of Mike McPhaden and two other anonymous reviewers considerably helped in improving the scientific content of the present study.

Appendix A

The heat equation in the ocean interior can be written:

$$\rho c_p \partial_t T = -\rho c_p \nabla_h \cdot (\bar{\mathbf{u}} T) - \rho c_p \partial_z (wT) - \rho c_p \partial_z (K_v \partial_z T) + Q_{NS} \delta(z) + Q_{SW} f(z) + \rho c_p A_H \Delta_H T \quad (\text{A1})$$

where ρ is the sea water density, c_p is the heat capacity, T is the temperature, $\bar{\mathbf{u}}$ is the horizontal currents, w is the vertical current, $\partial_z (K_v \partial_z T)$ represents the vertical turbulent flux, Q_{NS} is the non-solar component of the surface heat flux, $\delta(z)$ is a Dirac function equal to zero below the surface, Q_{SW} is the penetrating short-wave heat flux, $f(z)$ is a function describing the absorption of the short-wave heat flux and $A_H \Delta_H T$ is the horizontal diffusion of temperature (A_H being assumed vertically constant). By integrating Eq. (A1) over a time-dependent layer depth $h(t)$, and by introducing for each field (q) its average over the mixed-layer (q_a) and the deviation at each depth between the field value and its average ($q' = q - q_a$), the mixed-layer temperature equation becomes (see Stevenson and Niiler 1983; Vialard et al. 2000):

$$\begin{aligned} \partial_t T_a = & -\bar{u}_a \cdot \nabla T_a - \frac{1}{h} (T_a - T_{-h}) (\partial_t h + w_{-h}) + \frac{1}{h} (K_v \partial_z T)_{-h} \\ & + \frac{1}{h} \int_{-h}^0 \nabla_h \cdot (\bar{\mathbf{u}} T') dz + \frac{1}{h} (Q_{NS} + Q_{SW} I(-h)) \\ & + A_H \Delta_H T_a + \frac{1}{h} \int_{-h}^0 A_H \Delta_H T' dz \end{aligned} \quad (\text{A2})$$

where $I(-h)$ is the integrated value of $f(z)$ from the surface to the depth $-h$. It represents the percentage of the shortwave heat flux at the sea surface converted to thermal energy from the surface to depth $-h$.

Assuming that (1) $(K_v \partial_z T)_{-h} \approx K_v(-h) \frac{T_a - T_{-h}}{h}$, (2) $\frac{1}{h} \int_{-h}^0 \nabla_h \cdot (\bar{\mathbf{u}} T') dz$ is negligible, and (3) $\frac{1}{h} \int_{-h}^0 A_H \Delta_H T' dz$ is negligible, Eq. (A2) can be written:

$$\begin{aligned} \partial_t T_a = & -\bar{u}_a \cdot \nabla T_a - \frac{1}{h} (T_a - T_{-h}) (\partial_t h + w_{-h} + K_v/h) \\ & + \frac{1}{h} (Q_{NS} + Q_{SW} I(-h)) + A_H \Delta_H T_a \end{aligned} \quad (\text{A3})$$

First, $(\partial_t h + w_{-h})$ represents the entrainment/detrainment process induced by the variability of the mixed-layer depth and the vertical advection of temperature into the mixed-layer. When this term is positive, there is entrainment/advection of subsurface temperature into the mixed-layer which affects the mixed-layer temperature. When this term is negative, there is detrainment/advection of the mixed-layer temperature into the subsurface ocean. This process does not affect the mixed-layer temperature. Therefore, if, for the sake of simplicity, the sum of these two terms (mixed-layer change and vertical velocity) are grouped into w_{-h} , and if $(\partial_z T)_{-h} = \frac{1}{h} (T_a - T_{-h})$ represents the vertical gradient of temperature between the mixed-layer temperature (i.e. sea surface temperature) and the temperature at the base of the mixed-layer, the entrainment/detrainment/advection process can be rewritten: $-(\partial_z T)_{-h} M(w_{-h})$ where $M(x)$ is the step function equal to x if x is positive, to 0 otherwise. Then, dropping the subscript a in Eq. (A3), introducing for each field its climatolog-

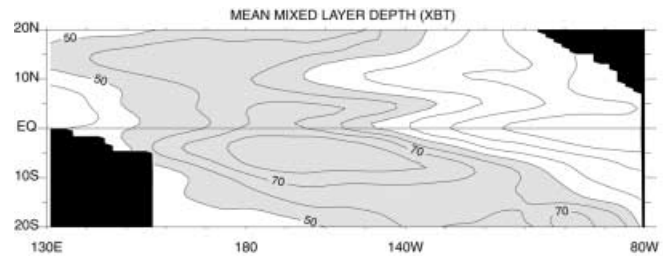


Fig. A1 Mean mixed-layer depth computed from TAO/XBT data over the period 1993–1996 (contours are every 10 m; values higher than 50 m are shaded)

ical component (\bar{q}) and the interannual variability ($q' = q - \bar{q}$), and noting $Q(-h)$ the total heat flux absorbed in the mixed-layer, it is straightforward to show that the interannual sea surface temperature equation is:

$$\begin{aligned} \partial_t T = & -(\bar{\mathbf{u}} \cdot \nabla T') - (\bar{\mathbf{u}}' \cdot \nabla (T + T')) \\ & - (M(\bar{w}_{-h} + w'_{-h}) - M(\bar{w}_{-h})) (\partial_z T) - M(\bar{w}_{-h} + w'_{-h}) (\partial_z T)' \\ & + (K_v/h) (\partial_z T)' + (K_v/h)' ((\partial_z T) + (\partial_z T)') \\ & + (Q(-h)/\rho_0 c_p h)' + A_H \Delta_H T' \end{aligned} \quad (\text{A4})$$

In the present work, we will consider the following hypotheses: (1) $(Q(-h)/\rho_0 c_p h)'$ is a negative feedback term simplified as $r_T T'$. Such an approximation is valid to some extent in the eastern Pacific but is not correct in the central Pacific where anomalous surface heat fluxes can reinforce the surface ocean heating (Seager 1989). (2) Following the basic assumption of the Zebiak and Cane (1987) model also used in various similar models (e.g. Battisti 1988; Chen et al. 1995; Dewitte 2000), the model mixed-layer depth is considered constant and equal to 50 m. As a consequence, the entrainment/detrainment process is not explicitly simulated by the model. Although such an approximation can induce large errors when simulating climatological SSTs especially in the eastern Pacific (Seager and Blumenthal 1994), intermediate models using this approximation have shown skills in simulating the Niño3 index on interannual time scales (Zebiak and Cane 1987). Relaxation of this approximation would require the use of a mixed-layer model which is beyond the scope of the present study. (3) The vertical diffusivity term K_v is often parametrized in terms of measured quantities using for instance a Richardson parametrization (Pacanowski and Philander 1981) or a turbulent kinetic energy (TKE) scheme (Gaspar et al. 1990; Blanke and Delecluse 1993). In the context of TKE, the model mixed-layer can be computed as the depth at which the coefficient K_v reaches a threshold value which can be chosen in a broad range 10^{-3} – 10^{-5} without significantly affecting the mixed-layer depth estimation as the value of K_v drops quickly below that depth. Using such a definition, the value of K_v at the base of the mixed-layer is taken constant in space and time. (4) Finally as our model does not simulate the mixed-layer depth variability, we will not take into account the time variations of $(1/h)$ or $(1/h)'$. As a consequence the third line of Eq. (A4) becomes $K_v(1/h(x, y)) (\partial_z T)'$ and we define $K_T(x, y) = K_v/h(x, y)$ where K_v is constant (which value, $5 \cdot 10^{-4}$, is discussed in Sect. 4) and $h(x, y)$ is the mean mixed-layer depth computed from TAO/XBT data (see Fig. A1). Further improvement of the model will require the development of a parametrization of the spatial and temporal evolution of the mixed-layer depth or the use of a sophisticated mixed-layer model. The final equation for SST anomalies is presented in Sect. 3.

References

- Battisti DS (1988) Dynamics and thermodynamics of a warming event in a coupled tropical atmosphere-ocean model. *J Atmos Sci* 45: 2889–2819

- Blanke B, Delecluse P (1993) Variability of the Tropical Atlantic Ocean simulated by a general circulation model with two different mixed-layer physics. *J Phys Oceanogr* 23: 1363–1388
- Boulanger J-P (2000) The Trident Pacific model. Part I: Simulating surface ocean currents with a linear model during the 1993–1998 TOPEX/POSEIDON period. *Clim Dyn* (this issue)
- Boulanger J-P, Menkes C (1999) Long equatorial wave reflection in the Pacific Ocean during the 1992–1998 TOPEX/POSEIDON period. *Clim Dyn* 15: 205–225
- Chen Y-Q, Battisti DS, Sarachik ES (1995) A new ocean model for studying the tropical oceanic aspects of ENSO. *J Phys Oceanogr* 25: 2065–2089
- Dewitte B (2000) Sensitivity of an intermediate ocean-atmosphere coupled model of the Tropical Pacific to its oceanic structure. *J Clim* 29: 1542–1570
- Gaspar P, Gregoris Y, Lefevre J-M (1990) A simple eddy-kinetic energy model for simulations of the ocean vertical mixing: tests at station Papa and Long-Term Upper Ocean Study Site. *J Geophys Res* 95: 16179–16193
- Harrison DE, Vecchi GA (1999) On the termination of El Niño. *Geophys Res Lett* 26: 1593–1596
- Hayes SP, Mangum LJ, Picaut J, Sumi A, Takeuchi K (1991) TOGA-TAO: a moored array for real-time measurements in the tropical Pacific ocean. *Bull Am Meteorol Soc* 72: 3339–3347
- Levitus S (1982) Climatological atlas of the world ocean. NOAA Prof Pap 13, US Government Printing Office Washington, D.C., USA, pp 183
- McPhaden MJ (1999) Genesis and evolution of the 1997–1998 El Niño. *Science* 283: 950–954
- McPhaden MJ (1993) TOGA-TAO and the 1991–93 El Niño–Southern Oscillation event. *Oceanography* 6: 36–44
- McPhaden MJ, Yu X (2000) Equatorial waves and the 1997–1998 El Niño. *Geophys Res Lett* (in press)
- Mantua NJ, Battisti DS (1994) Evidence for the delayed oscillator mechanism for ENSO: the “observed” oceanic Kelvin mode in the far western Pacific. *J Phys Oceanogr* 24: 691–699
- Pacanowski RC, Philander SGH (1981) Parametrization of vertical mixing in numerical models of tropical oceans. *J Phys Oceanogr* 11: 1443–1451
- Picaut J, Masia F, duPenhoat Y (1997) An advective-reflective conceptual model for the oscillatory nature of the ENSO. *Science* 277: 663–666
- Picaut J, Ioualalen M, Menkes C, Delcroix T, McPhaden MJ (1996) Mechanism of the zonal displacements of the Pacific warm pool: implications for ENSO. *Science* 274: 1486–1489
- Picaut J, Delcroix T (1995) Equatorial wave sequence associated with warm pool displacements during the 1986–1989 El Niño–La Niña. *J Geophys Res* 100: 18393–18408
- Schopf PS, Suarez MJ (1988) Vacillations in a coupled ocean-atmosphere model. *J Atmos Sci* 45: 549–566
- Seager R (1989) Modelling tropical sea surface temperature: 1970–1987. *J Phys Oceanogr* 19: 419–434
- Seager R, Blumenthal MB (1994) Modeling tropical sea surface temperature with satellite-derived solar radiative forcing. *J Clim* 7: 1943–1957
- Smith NR (1995) An improved system for tropical ocean subsurface temperature analyses. *J Atmos Oceanic Technol* 12: 850–870
- Smith NR, Meyers G (1996) An evaluation of XBT and TAO data for monitoring tropical ocean variability. *J Geophys Res* 101: 28489–28502
- Stevenson JW, Niiler PP (1983) Upper ocean budget during the Hawaii-to-Tahiti shuttle experiment. *J Phys Oceanogr* 13: 1894–1907
- Vialard J, Menkes C, Boulanger J-P, Delecluse P, Guilyardi E, McPhaden MJ (2000) Oceanic mechanisms driving the SST during the 1997–1998 El Niño. (in press)
- Weisberg RH, Wang C (1997) A western Pacific paradigm for the El Niño–Southern Oscillation. *Geophys Res Letters* 24: 779–782
- Wang W, McPhaden MJ (2000a) The surface layer heat balance in the equatorial Pacific ocean. Part I: mean seasonal cycle. *J Phys Oceanogr* (in press)
- Wang W, McPhaden MJ (2000b) The surface layer heat balance in the equatorial Pacific ocean. Part II: interannual variability. *J Phys Oceanogr* (accepted)
- Zebiak SE, Cane MA (1987) A model El Niño/Southern Oscillation. *Mon Weather Rev* 115: 2262–2278